Room Temperature Ferromagnetism in Dilute Iron-Doped Yttrium Aluminum Garnet Polycrystals

ARTICLE *in* THE JOURNAL OF PHYSICAL CHEMISTRY C · NOVEMBER 2009

Impact Factor: 4.77 · DOI: 10.1021/jp9011747

3 AUTHORS, INCLUDING:

Kiyoshi Nomura
Tokyo University of Science / Meiji University
228 PUBLICATIONS **1,596** CITATIONS

Room Temperature Ferromagnetism in Dilute Iron-Doped Yttrium Aluminum Garnet Polycrystals

Z. Németh,*,†,‡ K. Nomura,‡ and Y. Ito‡

Institute of Chemistry, Eötvös Loránd University, Pázmány P. s. 1/A, 1117 Budapest, Hungary, and School of Engineering, The University of Tokyo, 7-3-1 Hongo, Bunkyo-ku, Tokyo, 113-8656 Japan

Received: February 9, 2009; Revised Manuscript Received: September 22, 2009

Powder samples of $Y_3Al_{5-x}Fe_xO_{12}$ and $Y_3(YAl_{4-x})^BFe_xO_{12}$ garnets with iron concentrations between $0.02 \leq x \leq 0.4$ were investigated by means of magnetization measurements and Mössbauer spectroscopy. The results show that paramagnetism, antiferromagnetism, and ferromagnetism coexist in all samples at room temperature. The relative area of the ferromagnetic component was found to show a maximum at $x = 0.04$ and to diminish with raising the level of iron doping to $x \geq 0.1$. Postannealing the samples in air did not result in a significant alteration of the Mössbauer spectra, but it decreased the bulk ferromagnetism considerably due to elimination of oxygen vacancies. We propose that the induced ferromagnetism at low iron doping rates can be discussed in the frame of the dilute ferromagnetism model for insulators, and so iron-doped yttrium aluminum garnets may represent one of novel room temperature dilute ferromagnetic materials.

Introduction

The evolution of correlated electric and magnetic phenomena like superconductivity, giant-, and colossal magnetoresistance have boosted countless industrial application and stretched our basic knowledge of solid-state physics and chemistry during the recent decades. As one of the latest revelations, room temperature dilute ferromagnetism in semiconductors (DMS)[1–3] attracts considerable interest with its outstanding potential in spintronics. Besides the low-temperature DMS composites, like GaMnAs or InMnAs,[4] up to date results list slightly doped oxides (e.g., a few percent of Fe, Mn or Co ions in TiO_2, SnO_2, ZnO, CuO etc.)[1–3,5–9] and nitrides (as GaN)[10] as potential room temperature DMS candidates. Although the description of the roots of DMS effect is far from being satisfactory, several basic models have already been outlined.[11] Recently, Behan et al. proposed that a clear distinction should be made between dilute magnetic semiconductors and dilute magnetic insulators (DMI), as the mechanism behind their bulk magnetism may be essentially different.[12] With a minuscule concentration of mobile charge carriers, dilute magnetism in insulators may be a consequence of static magnetic polarons which consist of magnetic impurity atoms and trapped electrons in crystal defects.[15] On the other hand, in DMS systems charge carriers with relatively high concentration have itinerant character and contribute to the valence bands of the semiconductor host; moreover, the spin moment of the itinerant carriers are locally coupled to that of the doping magnetic ions.[16] It was also shown that the very same material can be tuned from DMI to DMS with altering the number of charge carriers via oxygen stoichiometry or additional doping with nonmagnetic atoms like Al.[12]

On the other hand, numerous reports describe the observed weak magnetization of the DMI or DMS candidates as a contribution of small magnetic particles or surface effects. For example, it is reported recently that nanoparticles of nonmagnetic oxides such as pure ZnO,[13] CeO_2, Al_2O_3, ZnO, In_2O_3, and SnO_2[14] show room temperature ferromagnetism with saturation magnetization of about $10^{-3}-10^{-4}$ emu/g. It was considered that the origin of ferromagnetism may be the exchange interactions between unpaired electron spins arising from oxygen vacancies at the surface of the nanoparticles.

Widening the spectrum of DMS and DMI materials is essential to test the applicability of current theories of dilute ferromagnetism. In this paper we argue that the observed room temperature bulk ferromagnetism in dilute iron-doped yttrium aluminum garnets may not arise due to ferromagnetic and antiferromagnetic interactions between neighboring iron ions like in $Y_3Fe_5O_{12}$ (YIG), but they may represent a new class of DMI oxides.

Sharing the same crystallographic structure (cubic garnets with an *Ia*3*d* space group[17]) YIG and $Y_3Al_5O_{12}$ (YAG) are both insulators but differ in their magnetic character. YIG is ferrimagnetic as the tetrahedral (d) and octahedral (a) sublattices occupied by magnetic Fe^{3+} ions (in 24:16 ratio) align antiferromagnetically.[17] Mössbauer studies revealed three magnetic components for YIG at room temperature, but the two subspectra of the octahedral sites differ only slightly[18,19] and in the case of any broadening they can be treated as one component.[20] The ideal crystal of YAG is diamagnetic and insulating due to the absence of both ions with unpaired electron spins and itinerant charge carriers.[21] However, real samples show weak mixed ionic-electronic conduction as a result of the presence of cation impurities and oxygen vacancies.[22]

Solid solutions of YIG and YAG have been successfully prepared over the entire composition range, but the question of site preference for Al and Fe is still dubious. Prediction,[17] theoretical calculation,[23] and X-ray and neutron diffraction experiments[24,25] indicated indirectly that smaller sized aluminum ions should prefer the smaller (d) sites, while iron ions the (a) ones. Despite that, direct observations with Mössbauer spectroscopy showed no change in the ratio of tetrahedral and octahedral iron ions in $Y_3Al_{5-x}Fe_xO_{12}$ compounds with changing x,[19,24,26,27] although in the case of high x all authors explained the observed broadening of the octahedral subspectrum and the

* To whom correspondence should be addressed. E-mail: hentes@chem.elte.hu.
† Eötvös Loránd University.
‡ The University of Tokyo.

10.1021/jp9011747 CCC: $40.75
Published on Web 10/26/2009

absence of broadening of the tetrahedral one with the assumption that all (a) sites are occupied by Fe while the (d) sites by both Al and Fe. It is worth noting that the theoretically calculated solution energy of Fe_2O_3 into $Y_3Al_5O_{12}$ crystals was found to be very similar for the cases when iron enters the tetrahedral or the octahedral sites,[23] which indicates that the level of Al−Fe cation disorder shall be very high.

In addition to mixing aluminum and iron in the (a) and (d) sites, oxygen nonstoichiometry and even cation impurities were reported to play significant role in the transport properties of garnets.[22] Besides enhancing ionic conductivity, oxygen vacancies were found to favor reduction of Fe^{3+} ions into Fe^{2+}, where the extra electrons can contribute to the itinerant charge carriers.[21,29–31] Moreover, divalent cation impurities were expected to provoke competition between formation of oxygen vacancies and oxidation of iron ions into Fe^{4+}.[22] However, Mössbauer spectra of $Y_3Al_{5-x}Fe_xO_{12}$ garnets presented only trivalent iron ions on both crystallographic sites.[18–20,24,26]

Bulk magnetization in $Y_3Al_{5-x}Fe_xO_{12}$ products were found to arise in the range of $2.5 \leq x \leq 5$ originating from the ferrimagnetic iron network. The Curie temperature decreases from 555 to 110 K with decreasing iron content between the above-mentioned extremes due to the diluting effect of nonmagnetic aluminum ions. Compositions of $x = 0.05$, 0.6, 0.8, and 1.2 were found to show only paramagnetism at room temperature.[27]

In the following we show an unprecedented iron-doping dependence of room temperature ferromagnetic signal in $Y_3Al_{5-x}Fe_xO_{12}$ ($x = 0.02$, 0.1) and $Y_3(YAl_{4-x})^BFe_xO_{12}$ ($x = 0.04$, 0.2, 0.4) samples prepared by sol−gel method and discuss it in the frame of dilute ferromagnetism.

Experimental Section

Two series of samples were prepared for the presented experiments. Both series were produced by the citrate sol−gel method as follows. First, citric acid and ethylene glycol were added to solutions of metal nitrates and ^{57}Fe chloride. The mixed solutions with nominal compositions were stirred and evaporated at 353 K, thermally decomposed at 573−723 K in air, and finally calcined at 1173 K for 3 h in air.

The first branch of samples was prepared with the nominal composition of $YAl_{1-y}Fe_yO_3$ ($y = 0.01$, 0.05, 0.1) expecting perovskite structure. However, the X-ray diffractograms of these samples (recorded at room temperature, using Cu Kα radiation) show a dominant garnet phase of $A_3B_5O_{12}$ without the sign of perovskite or any other impurity phases, except for a small amount (<5%) of monoclinic $Y_4Al_2O_9$ in the case of the $x = 0.2$ (where $x = 4*y$) sample at $2\theta = 30.7°$. It follows that while the A site is occupied only by yttrium the B sites should be shared by aluminum, iron, and yttrium ions giving a composition of $Y_3(YAl_{4-x})^BFe_xO_{12}$ ($x = 0.04$, 0.2, 0.4), where the B in the superscript indicates that (besides the x mol iron ions) 1 mol of Y and $4 - x$ mol of Al ions occupy the B sites in the garnet structure. Compared to the conventional $Y_3Al_{5-x}Fe_xO_{12}$ garnets, the presence of excess yttrium atoms increased the a cubic cell parameter with about 0.015 nm and altered the intensity ratios in the X-ray diffractograms.

The second group of samples with $x = 0.02$ and 0.1 and also a sample with no iron content ($Y_3Al_5O_{12}$) were fabricated by choosing the relative amount of the starting materials in accordance with the nominal garnet stoichiometry ($Y_3Al_{5-x}Fe_xO_{12}$). The resultant X-ray diffractograms show pure garnet phase in good agreement with the reference CIF file no. 2003066 (Figure 1).

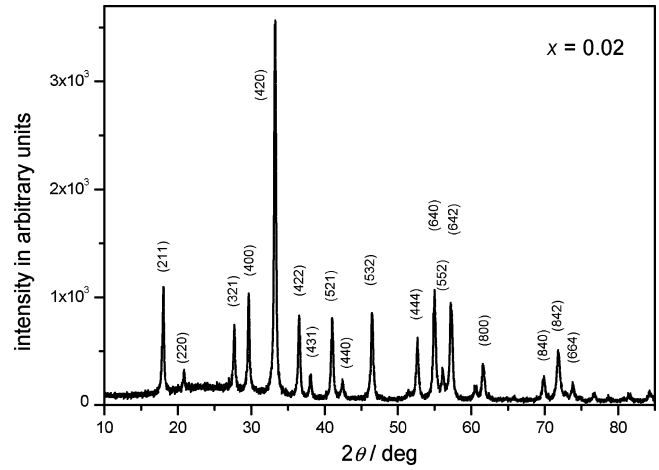

Figure 1. Example of the X-ray diffraction patterns recorded at room temperature: the $Y_3Al_{5-x}Fe_xO_{12}$ with $x = 0.02$ is shown. The *hkl* indexes of the peaks are displayed.

After the first series of measurements all five sample were postannealed at 1123 K during 1 h and then at 1223 K during 1 h in ambient atmosphere. The effect of heat treatment was investigated by X-ray diffractometry, Mössbauer spectroscopy, and magnetization measurements.

Mössbauer spectra were obtained by standard transmission geometry at room temperature and at 11 K. The γ-rays were provided by a $^{57}Co(Cr)$ source with an activity of 10^8 Bq. Isomer shifts are given relative to α-iron at room temperature. Magnetization measurements were carried out with a vibrating sample magnetometer (VSM, Riken Denshi Co., Ltd.) instrument at room temperature. Temperature dependency of magnetic properties with zero field cooling (ZFC) and field cooling (FC) modes were measured by a superconducting quantum interference device (SQUID) magnetometer.

Results

Although the iron-free $Y_3Al_5O_{12}$ sample, prepared by using the same conditions as in the case of the iron-doped samples, shows only the anticipated diamagnetic behavior (inset in Figure 2), bulk ferromagnetism was observed at room temperature in the samples with $x = 0.02$ and 0.04 among our investigated iron doped yttrium aluminum garnets. The room temperature magnetic hysteresis curves of all investigated iron containing samples show a dominant linear increase of magnetization with external magnetic field (up to $\mu_0 H = 0.5$ T), but the magnetization measurements hint also the presence of ferromagnetic order with a clearly observable hysteresis in the case of $x = 0.02$ and 0.04 (Figure 2). Although the observation of ferromagnetic signal could be interpreted by the presence of poorly crystallized magnetic impurities, invisible to the X-ray diffraction measurements, the disappearance of magnetic remanence and the abrupt decrease of magnetic moment per iron ion with increasing the iron content above $x > 0.1$ contradict the plausible expectation that more magnetic impurity should be formed with higher iron concentration. Moreover, although the measured magnetization per unit mass (in emu/g units) with $\mu_0 H = 0.5$ T applied magnetic field was found to increase with the iron content in both series of samples, these values belong to radically increasing number of doping magnetic iron ions, making the magnetization per magnetic iron ion in the $x = 0.02$ and 0.04 samples 10 times higher than those of $x > 0.1$. On the other hand, the diamagnetic iron-free sample proves that the exchange interactions between unpaired electron spins at oxygen vacancies

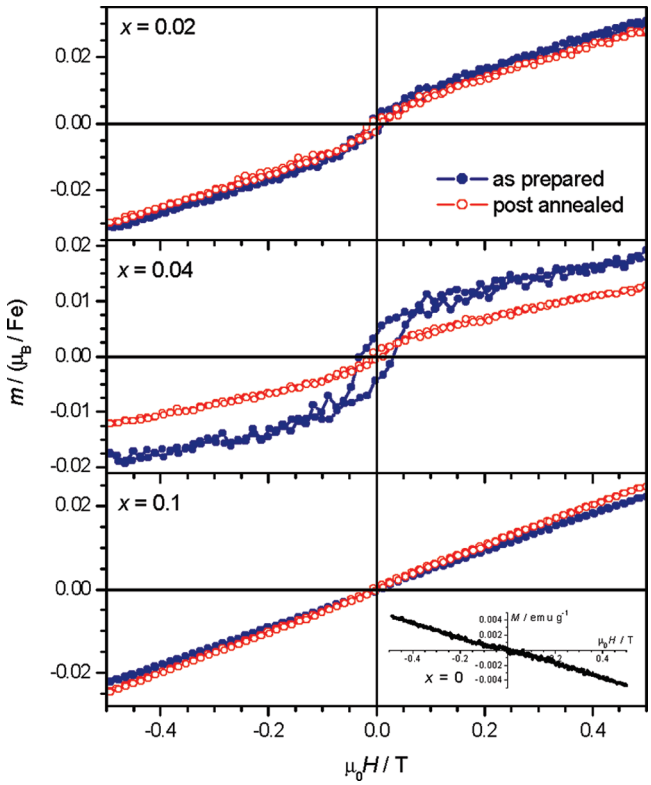

Figure 2. Room temperature magnetic hysteresis curves of $Y_3Al_{4.98}Fe_{0.02}O_{12}$, $Y_3(YAl_{3.96})^BFe_{0.04}O_{12}$, and $Y_3Al_{4.9}Fe_{0.1}O_{12}$ garnets before (full circles) and after (empty circles) the additional heat treatment in ambient atmosphere at 1123 K for 1 h and then at 1223 K for 1 h. The samples $x = 0.2$ and 0.4 show only paramagnetic linear $m-H$ curves both before and after the heat treatment. The inset of the bottom panel shows the diamagnetic behavior of the iron free YAG sample.

on the surface, described for nanosized diamagnetic materials as a source of bulk ferromagnetic signals,[14] also cannot be responsible for the measured ferromagnetic behavior in our case. These findings suggest the possibility of an alternative explanation of the observed bulk ferromagnetism in the presented iron-doped samples.

Comparing the two series of iron-doped samples, where the difference is that the B site in the garnet structure is occupied by x mol Fe and $5 - x$ mol of Al in the case of $x = 0.02$ and 0.1, while in the samples with $x = 0.04$, 0.2, and 0.4 x mol of Fe, 1 mol of Y, and $4 - x$ mol of Al are on the B sites, reveals that the magnetic susceptibility of the $Y_3(YAl_{4-x})^BFe_xO_{12}$ samples is significantly smaller than that of the $Y_3Al_{5-x}Fe_xO_{12}$ compounds; however, the disappearance of ferromagnetism with increasing the iron content above $x \geq 0.1$ (one of the major revelations of the present study) is a common feature.

Temperature dependence of DC magnetization of the examined $Y_3(YAl_{4-x})^BFe_xO_{12}$ garnets shows a dominant paramagnetic character for $x = 0.2$ and 0.4, but a complex magnetic structure for $Y_3(YAl_{3.96})^BFe_{0.04}O_{12}$. The ZFC and FC magnetization curves do not deviate from each other in the case of the samples with $x = 0.2$ and 0.4, and they can be satisfactorily fitted with the Curie−Weiss form of paramagnetism (inset of Figure 3). In contrast, in the case of $x = 0.04$ only the low temperature part (below around 50 K) follows the Curie−Weiss formula, while above 50 K the ZFC magnetization increases with temperature (Figure 3). The FC curve runs above the ZFC one, as the magnetization originating from room temperature induction with an $H = 50$ Oe external magnetic field does not disappear. This

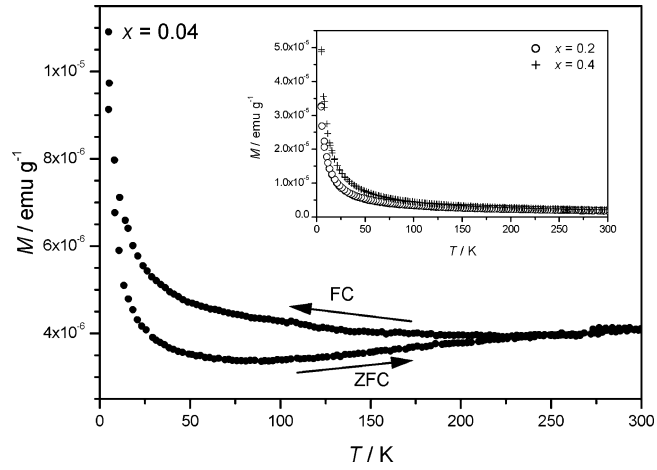

Figure 3. ZFC and FC magnetization curves of the $Y_3(YAl_{4-x})^BFe_xO_{12}$ samples. The main figure shows the temperature dependence of M_{ZFC} and M_{FC} for $x = 0.04$, while the inset demonstrates M vs T of $x = 0.2$ and 0.4. In the latter cases the field cooled and zero field cooled curves overlap. The applied magnetic field was 50 Oe.

behavior reflects a weak spin glass like magnetic state, that is, at the ZFC measurement the extra energy gained from the elevating temperature helps magnetic moments overcome the blocking magnetic couplings.

The room temperature Mössbauer spectra of the presented $Y_3Al_{5-x}Fe_xO_{12}$ and $Y_3(YAl_{4-x})^BFe_xO_{12}$ samples show three distinctive components in all five samples: the peaks at high velocities belong to two sextets with well developed magnetic order (marked with light gray filling in Figure 4); paramagnetic peaks at lower velocities refer to paramagnetic iron ions (gray subspectra in Figure 4), and the additional broad signal (shown only with a straight line) represents a wide distribution of hyperfine parameters. In general, with increasing the iron content from $x = 0.04$ the relative intensity of the sextets decreases at the expense of the paramagnetic doublets (Table 1), in the case of the $Y_3Al_{4.9}Fe_{0.1}O_{12}$ compound the amplitude of the sextet even hardly exceeds the detection limit. Although the relative area of the magnetic sextets correlates well with the intensity of the bulk ferromagnetic component, the sextets cannot originate from long-range ferromagnetic order but from antiferromagnetism because in the former case the bulk magnetization should be with order of magnitudes higher than the observed $m \approx 0.02$ μ_B/Fe atom values. However, this antiferromagnetic component cannot explain satisfactorily the presence and the iron doping dependence of the bulk ferromagnetic signal in the magnetization measurements. That is, in accordance with the results described in our recent article,[8] although the local magnetic order of the doping iron ions, reflected in the sextets in the Mössbauer spectra, may be in strong correlation with the bulk magnetism in the present samples, an additional component of ferromagnetic order can be presumed.

In order to analyze the nature of the broad component which exists besides the magnetic sextets and the paramagnetic doublets in all iron-doped samples, Mössbauer spectra were recorded at 11 K as well (Figure 5 shows the 11 K Mössbauer spectra of two selected samples). The low-temperature spectra of the samples with $x = 0.04$ and 0.2 were found to show the very same components as the corresponding room temperature ones, the only significant difference being the anticipated increase of isomer shifts and magnetic fields (Table 1). This outlines the possibility that the broad component observed at room temperature originates from relaxation of magnetic moments, as this feature should depend on the temperature

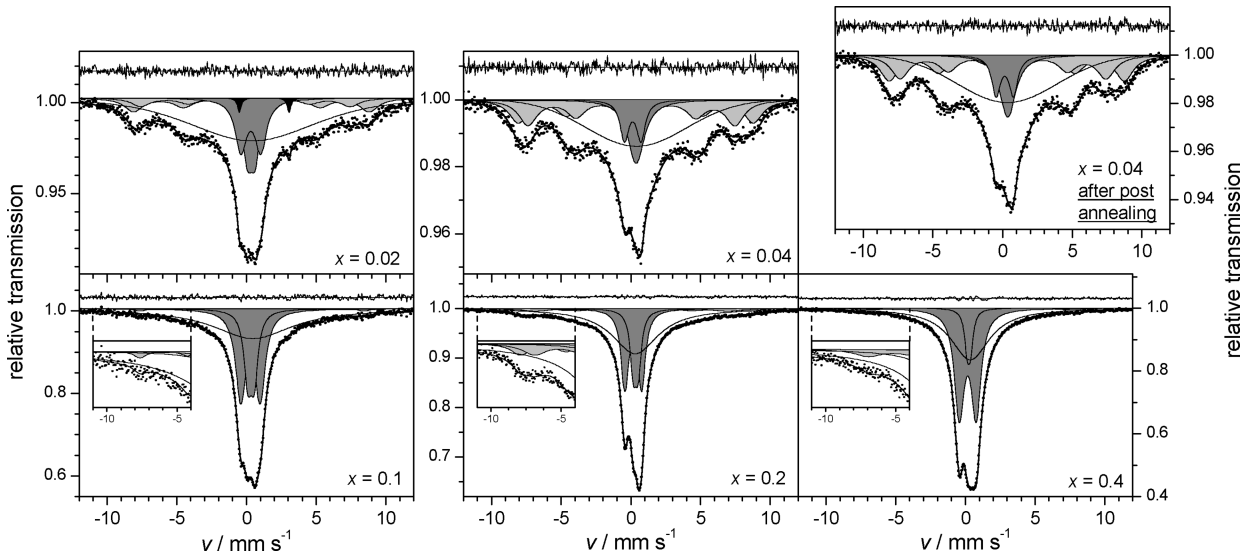

Figure 4. Room temperature ^{57}Fe Mössbauer spectra of $Y_3Al_{5-x}Fe_xO_{12}$ (left side) and $Y_3(YAl_{4-x})^BFe_xO_{12}$ (middle and right side) garnets. The insets show enlarged sections of some peaks corresponding to magnetic sextets (filled with light gray color).

TABLE 1: ^{57}Fe Mössbauer Parameters of $Y_3Al_{5-x}Fe_xO_{12}$ with (x = 0.02, 0.1) and $Y_3(YAl_{4-x})^BFe_xO_{12}$ (x = 0.04, 0.2, 0.4) Garnets[a]

	doublet 1			doublet 2			sextet 1				sextet 2				broad	
x	A/ %	δ/ mms^{-1}	Δ/ mms^{-1}	A/ %	δ/ mms^{-1}	Δ/ mms^{-1}	A/ %	δ/ mms^{-1}	B/ T	Δ/ mms^{-1}	A/ %	δ/ mms^{-1}	B/ T	Δ/ mms^{-1}	A/ %	δ/ mms^{-1}
0.02	12.7	0.34(1)	0.5(1)	14.2	0.31(1)	1.4(1)	7.2	0.05(9)	46.6(9)	−0.3(2)	11.7	0.36(5)	52.4(4)	−0.03(9)	52.9	0.42(5)
0.04	12.7	0.38(3)	0.2(8)	8.2	0.13(2)	1.19(4)	22.0	0.20(2)	46.0(3)	0.32(5)	20.0	0.32(3)	52.3(3)	0.07(5)	37.1	−0.41(4)
0.04[b]	5.4	0.40(1)	0.22(5)	14.7	0.29(1)	1.09(2)	25.4	0.25(2)	46.6(2)	−0.23(4)	18.9	0.46(1)	53.7(1)	−0.03(2)	35.6	0.61(5)
0.1	18.7	0.325(3)	0.46(1)	34.2	0.285(2)	1.39(1)	2.0	0.39(9)	49.8(7)	−	fitted together with sextet 1				45.1	0.46(3)
0.2	15.6	0.351(2)	0.344(3)	26.7	0.170(1)	1.205(2)	5.5	0.18(4)	43.1(6)	−0.24(8)	4.4	0.23(4)	50.9(5)	0.19(8)	47.8	0.311(8)
0.2[b]	25.3	0.45(1)	0.0(1)	24.7	0.263(5)	1.17(1)	5.4	0.22(9)	45(1)	−0.2(1)	6.8	0.46(8)	53.1(8)	−0.4(1)	37.9	0.40(4)
0.4	8.3	0.245(2)	0.242(5)	44.0	0.166(1)	1.210(4)	3.4	0.38(9)	45.5(8)	−	fitted together with sextet 1				44.3	0.35(1)

[a] A denotes relative area of subspectra, while δ, Δ, and B shows isomer shift, quadrupole splitting, and magnetic induction, respectively. The sextets were fitted with a linear first-order mixed magnetic + quadrupole model built in the MossWinn 3.0 software.[34] The parameters of the Fe^{2+} component of the x = 0.02 sample are the following. A = 1.2%, δ = 1.27(2) mm/s, Δ = 3.57(4) mm/s. [b] ^{57}Fe Mössbauer parameters of $Y_3(YAl_{4-x})^BFe_xO_{12}$ garnets recorded at 11 K.

TABLE 2: Room Temperature ^{57}Fe Mössbauer Parameters of $Y_3Al_{5-x}Fe_xO_{12}$ with (x = 0.02, 0.1) and $Y_3(YAl_{4-x})^BFe_xO_{12}$ (x = 0.04, 0.2, 0.4) after the Annealing Treatment (See Text)[a]

	doublet 1			doublet 2			sextet 1				sextet 2				broad	
x	A/ %	δ/ mms^{-1}	Δ/ mms^{-1}	A/ %	δ/ mms^{-1}	Δ/ mms^{-1}	A/ %	δ/ mms^{-1}	B/ T	Δ/ mms^{-1}	A/ %	δ/ mms^{-1}	B/ T	Δ/ mms^{-1}	A/ %	δ/ mms^{-1}
0.02	21.7	0.35(1)	0.65(3)	11.3	0.32(1)	1.58(7)	12.0	0.16(3)	46.4(2)	−0.41(1)	14.7	0.35(2)	53.0(3)	0.0(1)	38.4	0.34(4)
0.04	11.8	0.37(2)	0.2(3)	8.3	0.16(2)	1.23(4)	19.9	0.21(2)	45.8(1)	−0.35(4)	21.9	0.30(1)	52.3(2)	0.0(1)	38.0	0.34(3)
0.1	26.4	0.324(3)	0.53(1)	27.3	0.289(3)	1.46(1)	1.8	0.39	49.8		fitted together with sextet 1				44.4	0.41(3)
0.2	9.4	0.326(3)	0.322(1)	23.6	0.177(2)	1.234(5)	7.2	0.20(5)	42(1)	−0.7(8)	5.8	0.24	51.7(7)	0.09(7)	53.9	0.30(1)
0.4	5.6	0.23(1)	0.25(1)	45.7	0.176(3)	1.243(5)	5.5	0.2(2)	45(1)		fitted together with sextet 1				43.1	0.35(2)

[a] The heading of the table is the same as in Table 1.

strongly, and at 11 K the broad signal should transform into a sextet with clearly distinguishable peaks. However, this is not the case, which implies that the source of this component is more likely a structural inhomogeneity, which does not depend on the temperature.

After the samples were annealed at 1123 and 1223 K for 1 h at each temperature in ambient atmosphere, room temperature magnetization hysteresis and Mössbauer spectra have been recorded again. While the Mössbauer spectra of the five iron doped samples show no significant deviation from those measured before the heat treatment (the example for x = 0.04 is given in Figure 4, while the parameters are given in Table 2), the magnetic hysteresis of the $Y_3Al_{4.95}Fe_{0.02}O_{12}$ and the $Y_3(YAl_{3.96})^BFe_{0.04}O_{12}$ samples decreased remarkably (Figure 2), giving a strong emphasis that the bulk ferromagnetic signal of these samples cannot be solely connected to the magnetic iron ions but an additional source of the ferromagnetic order should be taken into consideration. Were the bulk ferromagnetic signal originated from iron containing magnetic impurities, the pronounced decrease of the ferromagnetic signal must have been appeared in the Mössbauer spectra as a strong decrease of a ferromagnetic sextet or the broad component, which was not observed.

Discussion

Two magnetic and two paramagnetic Fe^{3+} components can be found in all Mössbauer spectra reported hereby (although in

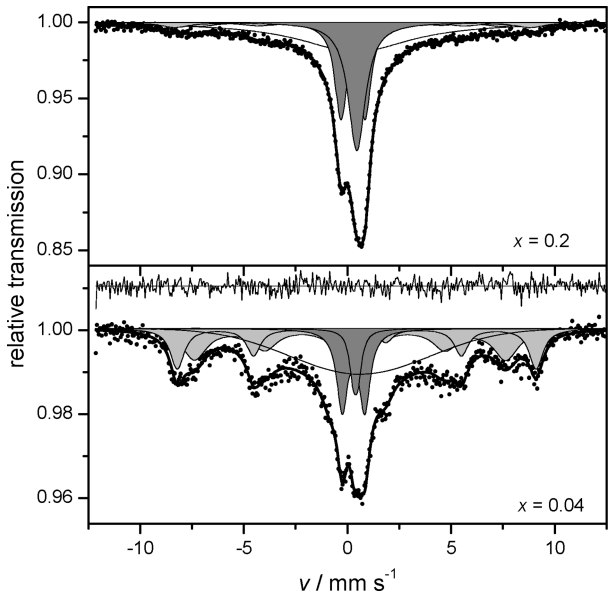

Figure 5. ^{57}Fe Mössbauer spectra of $Y_3(YAl_{3.96})^BFe_{0.04}O_{12}$ and $Y_3(YAl_{3.8})^BFe_{0.2}O_{12}$ garnets measured at 11 K.

the case of $x = 0.1$ and 0.4 the amplitude of the two sextets is too small to distinguish them). Comparing the fitted room temperature Mössbauer parameters (Table 1) with literature data,[18,19] the two magnetic sextets refer to iron ions in tetrahedral and octahedral sites, while the magnetic splitting of these Mössbauer subspectra shows that these iron ions can build up an antiferromagnetic phase, that is, it should refer to a relatively iron rich part of the samples. In our case, however, both sextets show considerably higher magnetic inductions (in average $B_{(d)} = 46$ T and $B_{(a)} = 52$ T) as compared to those found in the YIG samples being around $B_{(d)} = 40$ T and $B_{(a)} = 49$ T.[18–20] This difference suggests that in the case of the dilute iron doped garnets the source of magnetism should differ from the conventional ferrimagnetism in YIG. The two Fe^{3+} doublets can be assigned to paramagnetic iron ions in different crystallographic sites with no iron ions nearby, although the presence of oxygen vacancies or cation disorder can also alter the Mössbauer parameters significantly.

The observation of frozen magnetic disorder (spin glass like state) with the help of the temperature-dependent magnetization measurements (Figure 3) can explain the origin of the broad component in the Mössbauer spectra. Magnetically ordered regions, which are smaller than the optimal domain size (superparamagnetic domains), are ideal candidates for frustrated magnetic interactions, and thus they can form a spin glass like state. In a Mössbauer spectrum this state is reflected as a wide, complex peak like in our measurements. Although the broad component in the Mössbauer spectra occurs in the samples with high iron dopings ($x \geq 0.1$), as well, they are much narrower than those in the samples with low iron content, which may originate the disappearance of spin glass like behavior in the temperature dependent magnetization measurements.

The change of the bulk ferromagnetic order's extent with iron doping and postannealing, observed in the magnetic hysteresis curves (Figure 2), and the absence of clear correlation between local magnetic order of iron ions and the bulk magnetism suggests that the mechanism corresponding to the bulk ferromagnetic order in these dilute garnets is not likely to be explained with the ferromagnetic and antiferromagnetic interactions between neighboring magnetic iron ions only, as was shown, e.g., for iron-doped SnO_2[8]. Instead, the model of dilute ferromagnetism in DMI materials seems to give reasonable description of the present case. That is, the existence of overlapping locally bound polarons, consisting of doping magnetic iron ion(s) and a trapped donor electron (often called as magnetic defect), should result in the observed bulk ferromagnetism.[15] As it was described theoretically,[28] vacancies in the crystal structure can have partially occupied electronic levels within the band gap, and so they can carry a local magnetic moment. With usual preparation conditions the number of such magnetic vacancies is not enough to induce bulk ferromagnetism[28] (bulk FM appears only in the case of undoped nanoparticles with relatively huge surface[14]), but they can interplay with the magnetic moment of neighboring iron ions, forming magnetic polarons. Although it could be assumed that the ferromagnetic signal may occur due to clustering of an iron-rich ferrimagnetic phase, too, the probability of the formation of such a phase should be much higher in the case of the samples with higher iron doping levels, which mismatches, although not unambiguously contradicts our results.

While the iron-free YAG showed only diamagnetic property, with introducing 0.4% iron atoms at the Al sites the clear ferromagnetic signal may appear due to the formation of these magnetic polarons. Increasing the iron level slightly ($x = 0.04$), we have found that ferromagnetism gains further weight, which can be understood as the polarons grow in number and thus they have more possibility to coalesce and to build up long-range ferromagnetism as described in ref 15. The increasing number of coalesced magnetic polarons due to increasing the iron doping level may be reflected, although not directly, in the increasing relative area of the Mössbauer sextets. However, as the level of iron doping grows even further, the probability of iron−iron neighborhood increases drastically. This introduces direct magnetic coupling between the adjacent Fe ions and so it weakens the interaction between the magnetic polarons, leading to the suppression of bulk ferromagnetism, as seen in our measurements.

As was depicted in the model phase diagram of polaronic dilute magnetism,[15] bulk ferromagnetic order in dilute insulators occurs only in an optimal concentration range of both doping magnetic ions and defects. After investigating the effect of varying the iron concentration, we tried to alter the number of oxygen vacancies by postannealing as well. According to our recent results,[8] the present finding that during heat treatment the bulk magnetization changed but the Mössbauer spectra did only in an insignificant amount is a strong argument for that the bulk magnetization should originate indeed from magnetic defects and not form iron oxide clusters or any other magnetic impurities. These defects are, i.e., modulated by the change of oxygen stoichiometry, which was modified by the annealing process. In the polaronic model of DMI materials tuning the number of oxygen vacancies results in the change of the number of trapped charge carriers, which should affect indeed the number or connectivity of magnetic polarons, and thus the bulk magnetization.[12] On the other hand, the fact that the Mössbauer spectra did not reveal any significant change during the heat treatment shows that those oxygen vacancies were most likely eliminated by postannealing which were not adjacent to iron ions but only connected the existing magnetic polarons. That is, the annealing seems to prefer the fill up of the oxygen defects in the vicinity of Al ions but not next to the Fe atoms. Therefore, in contrast with the effect of iron doping, where the Mössbauer spectra changed with the increasing number of magnetic polarons due to the increasing number of iron ions, decreasing

the number of oxygen vacancies in the vicinity of Al ions may not affect the local environment of the Mössbauer active iron atoms.

Moreover, we ruled out the above-depicted model of DMS, as the number of charge carriers should be very small in our system. This assumption is based on the fact that the Mössbauer spectra show only trivalent iron ions with isomer shifts (δ) between 0.1 and 0.4 mm/s, except of a tiny (with a relative area of 1.2%) doublet of Fe^{2+} in the case of the $x = 0.02$ sample (Table 1). However, it was shown that the only possible source of electronic conduction is excess electrons originated from oxygen vacancy in $Y_3Al_{5-x}Fe_xO_{12}$ garnets. As these electrons favor occupying an empty iron 3d orbital,[21,29–31] they should increase the isomer shift values noticeably. In the bound polaron model, which was derived for the DMI materials and also outlined for the case of the present samples in the previous paragraph, the locally trapped electrons do not affect much the electronic state of iron ions as seen by Mössbauer spectroscopy.

Conclusions

Investigating the room temperature magnetic properties of $Y_3Al_{5-x}Fe_xO_{12}$ and $Y_3(YAl_{4-x})^BFe_xO_{12}$ garnets with $x = 0$, 0.02, 0.1 and $x = 0.04$, 0.2, 0.4, respectively, unexpected ferromagnetism was found, which shows a maximum at $x = 0.04$ and diminishes with increasing the iron doping ratio until $x = 0.4$. The occurrence of the ferromagnetic character was discussed in frame of the recently depicted scenario for dilute ferromagnetic insulators. It was found that the ferromagnetism of the $Y_3Al_{4.95}Fe_{0.02}O_{12}$ and the $Y_3(YAl_{3.96})^BFe_{0.04}O_{12}$ samples becomes weaker by annealing at high temperatures. Oxygen vacancy was considered to induce room temperature ferromagnetism through the iron ions and trapped polarized electrons in the investigated dilute YAG garnets.

Acknowledgment. The authors express their gratefulness to the Matsumae International Foundation for supporting Z.N. for his stay in Tokyo for collaboration. Y.I. is a visitor from the Tokyo University of Science. The authors are also thankful for the valued help of Dr. H. Takagi and Mr. K. Kuwano.

References and Notes

(1) Matsumoto, Y.; Murakami, M.; Shono, T.; Hasegawa, T.; Fukumura, T.; Kawasaki, M.; Ahmet, P.; Chikyow, T.; Koshihara, S.; Koinuma, H. *Science* **2001**, *291*, 854.

(2) Janisch, R.; Gopal, P.; Spaldin, N. A. *J. Phys.: Condens. Matter* **2005**, *17*, R657.

(3) Liu, C.; Yun, F.; Morkoc, H. *Mater. Sci.: Mater. Electron.* **2005**, *16*, 555.

(4) See, e.g., Jungwirth, T.; Sinova, J.; Mašek, J.; Kučera, J.; MacDonald, A. H. *Rev. Mod. Phys.* **2006**, *78*, 809, and references within.

(5) Sharma, P.; Gupta, A.; Rao, K. V.; Owens, F. J.; Sharma, R.; Ahuja, R.; Osorio Guillen, J. M.; Johansson, B.; Gehring, G. A. *Nat. Mater.* **2003**, *2*, 673.

(6) Liu, C.; Yun, F.; Morkoc, H. *J. Mater. Sci.-Mater. Electron.* **2005**, *16*, 555.

(7) Zhao, F.; Qiu, H. M.; Pan, L. Q.; Zhu, H.; Zhang, Y. P.; Guo, Z. G.; Yin, J. H.; Zhao, X. D.; Xiao, J. Q. *J. Phys.: Condens. Matter* **2008**, *20*, 425208.

(8) Nomura, K.; Barrero, C. A.; Sakuma, J.; Takeda, M. *Phys. Rev. B* **2007**, *75*, 184411.

(9) Rykov, I.; Nomura, K.; Sakuma, J.; Barrero, C. A.; Yoda, Y.; Mitsui, T. *Phys. Rev. B* **2008**, *77*, 014302.

(10) Larson, P.; Popović, Z. S.; Satpathy, S. *Phys. Rev. B* **2008**, *78*, 113308.

(11) Coey, J. M. D.; Wongsaprom, K.; Alaria, J.; Venkatesan, M. *J. Phys. D: Appl. Phys.* **2008**, *41*, 134012.

(12) Behan, A. J.; Mokhtari, A.; Blythe, H. J.; Score, D.; Xu, X.-H.; Neal, J. R.; Fox, A. M.; Gehring, G. A. *Phys. Rev. Lett.* **2008**, *100*, 047206.

(13) Gao, D.; Zhang, Z.; Fu, J.; Xu, Y.; Qi, J.; Xue, D. *J. Appl. Phys.* **2009**, *105*, 113928.

(14) Sundaresan, A.; Bhargavi, R.; Rangarajan, N.; Siddesh, U.; Rao, C. N. R. *Phys. Rev. B* **2006**, *74*, 161306.

(15) Coey, J. M. D.; Venkatesan, M.; Fitzgerald, C. B. *Nat. Mater.* **2005**, *4*, 173.

(16) Chattopadhyay, A.; Das Sarma, S.; Millis, A. J. *Phys. Rev. Lett.* **2001**, *87*, 227202.

(17) Gilleo, M. A.; Geller, S. *Phys. Rev.* **1958**, *110*, 73.

(18) van Loef, J. J. *J. Appl. Phys.* **1968**, *39*, 1258.

(19) Sauer, Ch.; Zinn, W.; Tolksdorf, W. *IEEE Trans. Magn.* **1978**, *14*, 701.

(20) Nomura, K.; Hanai, T.; Sadamoto, R.; Ujihira, Y.; Ryuo, T.; Tanno, M. *Hyperfine Interact.* **1994**, *84*, 421.

(21) Milanese, C.; Buscaglia, V.; Maglia, F.; Anselmi-Tamburini, U. *Chem. Mater.* **2004**, *16*, 1232.

(22) Rotman, S. R.; Tuller, H. L. *J. Electroceram.* **1998**, *2*, 95.

(23) Maglia, F.; Buscaglia, V.; Gennari, S.; Ghigna, P.; Dapiaggi, M.; Speghini, A.; Bettinelli, M. *J. Phys. Chem. B* **2006**, *110*, 6561.

(24) Kim, C. S.; Min, B. K.; Kim, S. J.; Yoon, S. R.; Uhm, Y. R. *J. Magn. Magn. Mater.* **2003**, *254*−*255*, 553.

(25) Rodic, D.; Mitric, M.; Tellgren, R.; Rudlof, H. *J. Magn. Magn. Mater.* **2001**, *232*, 1.

(26) Thongmee, S.; Winotai, P.; Tang, I. M. *Solid State Commun.* **1999**, *109*, 471.

(27) Chen, Y. F.; Wu, K. T.; Yao, Y. D.; Peng, C. H.; You, K. L.; Tse, W. S. *Microelectron. Eng.* **2005**, *81* (2005), 329.

(28) Osorio-Guillén, J; Lany, S.; Barabash, S. V.; Zunger, A. *Phys. Rev. B* **2007**, *75*, 184421.

(29) Masumoto, T.; Kuwano, Y. *Jpn. J. Appl. Phys.* **1985**, *24*, 546.

(30) Chen, C. Y.; Pogatshnik, G. J.; Chen, Y. *Phys. Rev. B* **1988**, *38*, 8555.

(31) Akhmadullin, I.; Golenischev-Kutuzov, V.; Migachev, S.; Korzhik, M. *J. Phys. Chem. Solids* **1993**, *54*, 117.

(32) Medraj, M.; Hammond, R.; Parvez, M. A.; Drew, R. A. L.; Thompson, W. T. *J. Eur. Ceram. Soc.* **2006**, *26*, 3515.

(33) Grasset, F.; Mornet, S.; Demourgues, A.; Portier, J.; Bonnet, J.; Vekris, A.; Duguet, E. *J. Magn. Magn. Mater.* **2001**, *234*, 409.

(34) Klencsár, Z.; Kuzmann, E.; Vértes, A. *J. Radioanal. Nucl. Chem.* **1996**, *210*, 105.

JP9011747